Evolution of gravity-driven rock slope failure and associated fracturing: Geological analysis and numerical modelling

S. Bouissou *, R. Darnault, A. Chemenda, Y. Rolland

Université de Nice Sophia-Antipolis, Observatoire de la Côte d'Azur, Laboratoire Géoazur, UMR 6526, 250 rue A. Einstein, 06560 Valbonne, France

ARTICLE INFO

ABSTRACT

An accurate analysis of fracture and cleavage anisotropies along two landslides in the Argentera massif (French Southern Alps) was performed in order to relate the fracturing mode to the rock slope failure state. The mature La Clapière landslide and the incipient Isola Landslide were investigated. In both cases, the gneissic rock schistosity was found sub-horizontal in the vicinity of the landslides at shallow depths, while it was sub-vertical elsewhere at the massif's scale. In addition to the well known regional tectonic fracture sets, we identified in both cases a new family of vertical valley parallel (VP) fractures. The VP fractures were only observed on the lower part of slopes affected by landslides where schistosity was found sub-horizontal. The VP fractures are clearly related to the decrease in schistosity dip and correspond to 'fold extrado'-like joints. The proximity of the schistosity folds and the associated VP joints to the landslides suggests that they are gravity-driven. The presented 2-D finite-difference models of the slope destabilisation in the La Clapière site shade light on possible mechanisms of the indicated gravity-induced processes. A progressive degradation of the material strength was imposed in these models to simulate the weathering effect which led to inelastic deformation/damage at the lower part of slope. This was followed by the formation of dense sub-vertical deformation bands and then by the initiation of a landslide in the area corresponding to the actual position of the La Clapière landslide. It is suggested that the gravity-induced damage in the lower part of slope increases the permeability and thereby accelerates the weathering that causes a more rapid strength reduction. The latter results in the tilting/folding of pre-existing fabrics and the related VP fracturing. The La Clapière landslide is initiated in the upper part of this zone.

© 2011 Elsevier B.V. All rights reserved.

1. Introduction

Gravitational slope failure is known to be influenced by several factors among which the structural heterogeneities and alteration/weathering processes are assumed to play a dominant role. Both physical and chemical weathering and alteration are caused by temperature changes and fluid circulations within the fractures and pores (Hall and André, 2001; Hoek and Brown, 1997; Migon and Lidmar-Bergstroem, 2002). Slope movements develop largely through the propagation and interaction of pre-existing fractures of tectonic origin (Bois and Bouissou, 2010; Bois et al., 2008; Kaneko et al., 1997; Scavia, 1995) and the development of new gravity-induced fractures (Bachmann et al., 2009; Petley, 1996). The relative influence of the listed factors is still misunderstood, which requires further investigations. In this work we performed a geological analysis and numerical modelling of the Argentera massif (French Southern Alps) along the Tinée valley. The eastern side of the valley is subjected to active landsliding and is composed of weathered metamorphic units affected by tectonic fracture sets related to the Oligocene–Miocene thrust

tectonics (Gunzburger and Laumonier, 2002). In order to analyze the evolution of fracturing during gravitational rock slope failure we carried out an accurate analysis of fractures and cleavage anisotropies along the slope (from the toe to the crest) around two landslides, the mature La Clapière landslide active for about sixty years (Casson et al., 2005; Follacci, 1987, 1999; Guglielmi et al., 2002) and the initiating Isola landslide. In both cases, the schistosity was found sub-horizontal in the vicinity of the landslides at shallow depth and sub-vertical elsewhere. In addition to the well known tectonic fracture sets, we documented in both cases a new family of vertical, valley parallel (VP) fractures. The latter are 'fold extrado'-like joints associated with a progressive tilting of schistosity. The proximity of this schistosity folding and the VP jointing to the landslides suggests that they are gravity-induced.

The presented finite-difference models support this conclusion. The principal factor defining the gravity-driven destabilization of the model was a gradual reduction of the cohesion simulating effects of alteration/weathering. This corresponds to a time softening of the material and not to a strain softening applied in some other studies (Eberhardt et al., 2004; Hajiabdolmajid and Kaiser, 2002). The modelling approach is similar to that reported in Chemenda et al. (2009), where we investigated a large-scale (relatively low-resolution) gravity induced deformation pattern and related landsliding in the La Clapière area. A simple Hooke–Mohr–Coulomb constitutive model was used
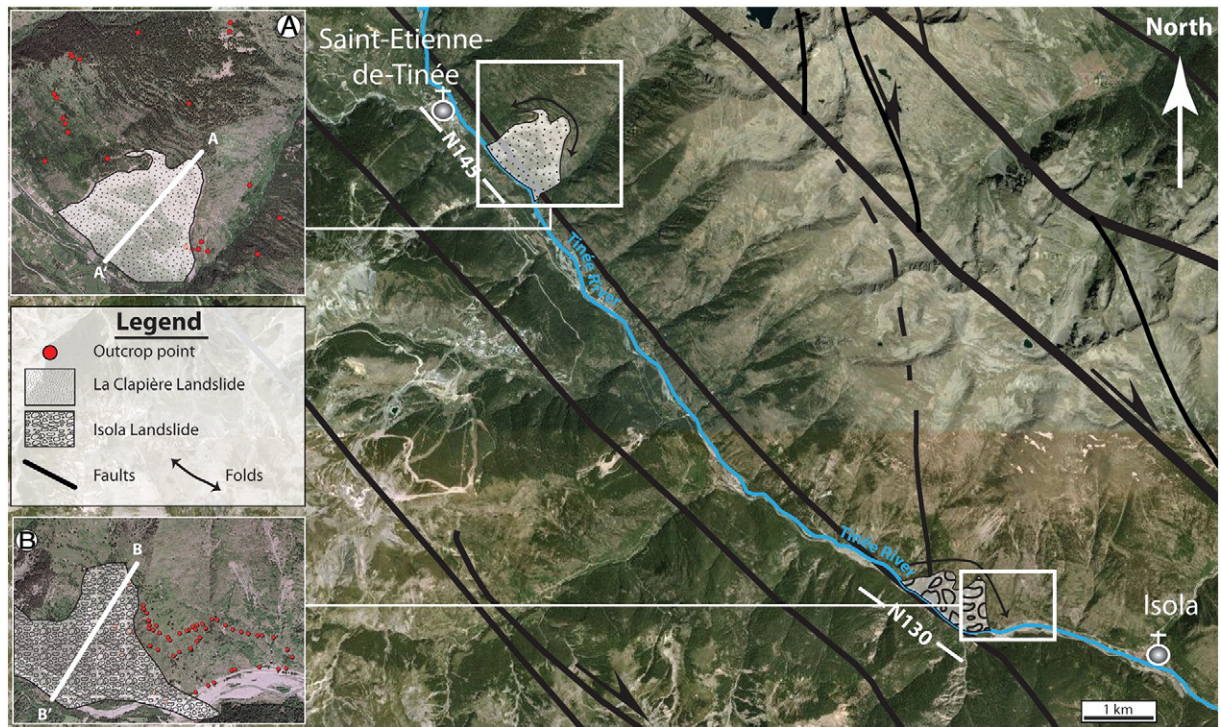
Fig. 1. Simplified structural map of the study area. The squares (a) and (b) show the La Clapière and Isola landslides, respectively. Outcrop points in red show the zones where measurements have been performed. The segments AA′ and BB′ are the traces of cross sections shown in Figs. 3 and 5, respectively.

with different boundary conditions, model size, and resolution. In all cases the model evolution leads to inelastic deformation that at later stages can localize into sub-vertical shear bands, which follows by landsliding in the upper part of the damaged (inelastically deformed) volume.

2. Geological setting

2.1. General framework

The study area is located in the Tinée valley, southern French Alps, at the north-western edge of the Argentera-Mercantour massif (Fig. 1). The latter corresponds to a wide outcrop of Hercynian 300–320 Ma metamorphic rocks (mainly micaschists and gneiss) with steeply dipping schistosity planes trending N 150°E (Bogdanoff, 1986; Delteil et al., 2003). Several sets of dextral N140°E mylonitic shear zones crosscut the entire massif. They were formed at mid-crustal depth conditions between 32 and 20 Ma (Corsini et al., 2004; Sanchez et al., 2011a). Exhumation of this mid-crustal basement occurred in a mainly transpressive context during the last 20 Ma (Bigot-Cormier et al., 2005; Sanchez et al., 2011b). During exhumation, brittle deformation reactivated the former Hercynian or Alpine shear zones, and contributed to the basement fracturing. Symmetrical, decimeter-size conjugate shear fractures forming tectonic wedges and associated extension fractures have been identified (Gunzburger and Laumonier, 2002). For most wedges, fractures are oriented N115°E, 80°SW on average but also N70°E, 80°NW or N30°E, 80°NW. Related kinematics are right-lateral on N115°E planes and extensional + sinistral on the N30°E planes (Sanchez et al., 2010a). Deeply incised valleys in the region create optimal conditions for landsliding. About 30 landslides with mobilized volumes ranging from 5×10^6 to 60×10^6 m³ have been documented in the valley (El Bedoui et al., 2011; Jomard, 2006; Sanchez et al., 2010b). Among them, La Clapière landslide is located less than 1 km downstream Saint-Etienne-de-Tinée village (Fig. 1). This landslide extends over a width of 800 m at hillside foot to a 120 m high scarp at an elevation of 1600 m. The failure surface depth ranges from 100 m to 200 m (Guglielmi et al., 2005). The landslide moves downward at a rate

varying from 50 to 500 cm/yr (the average rate is of about 1 cm/day) (Casson et al., 2005; Jomard, 2006).

The Isola landslide is located at about 10 km from the La Clapière Landslide and at 1 km from the village of Isola (Fig. 1). This latter landslide corresponds mainly to superficial rock falls. It extends over a width of 1500 m at hillside foot to a 500 m high scarp at an elevation of 1200 m.

2.2. Characterisation of cleavage anisotropies and fracture sets

The La Clapière and Isola landslides areas were chosen for several reasons: i) they are among the largest active landslides of the Tinée
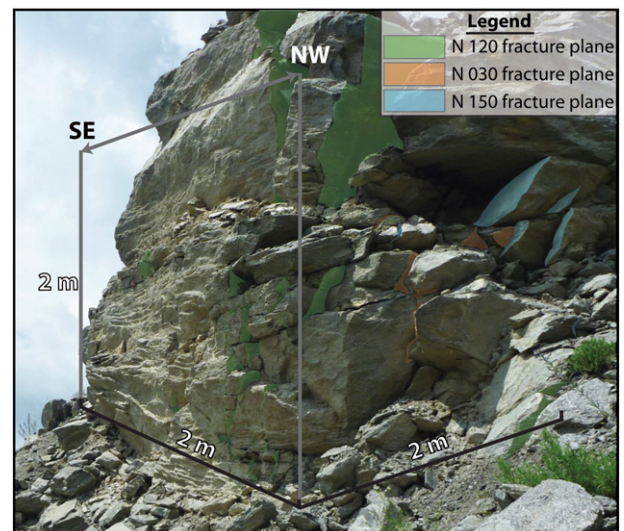
Fig. 2. Photo showing a representative outcrop for the structural measurements. The green, orange and blue colours highlight the fracture planes with an orientation of N120°E, N030°E and N150°E, respectively.
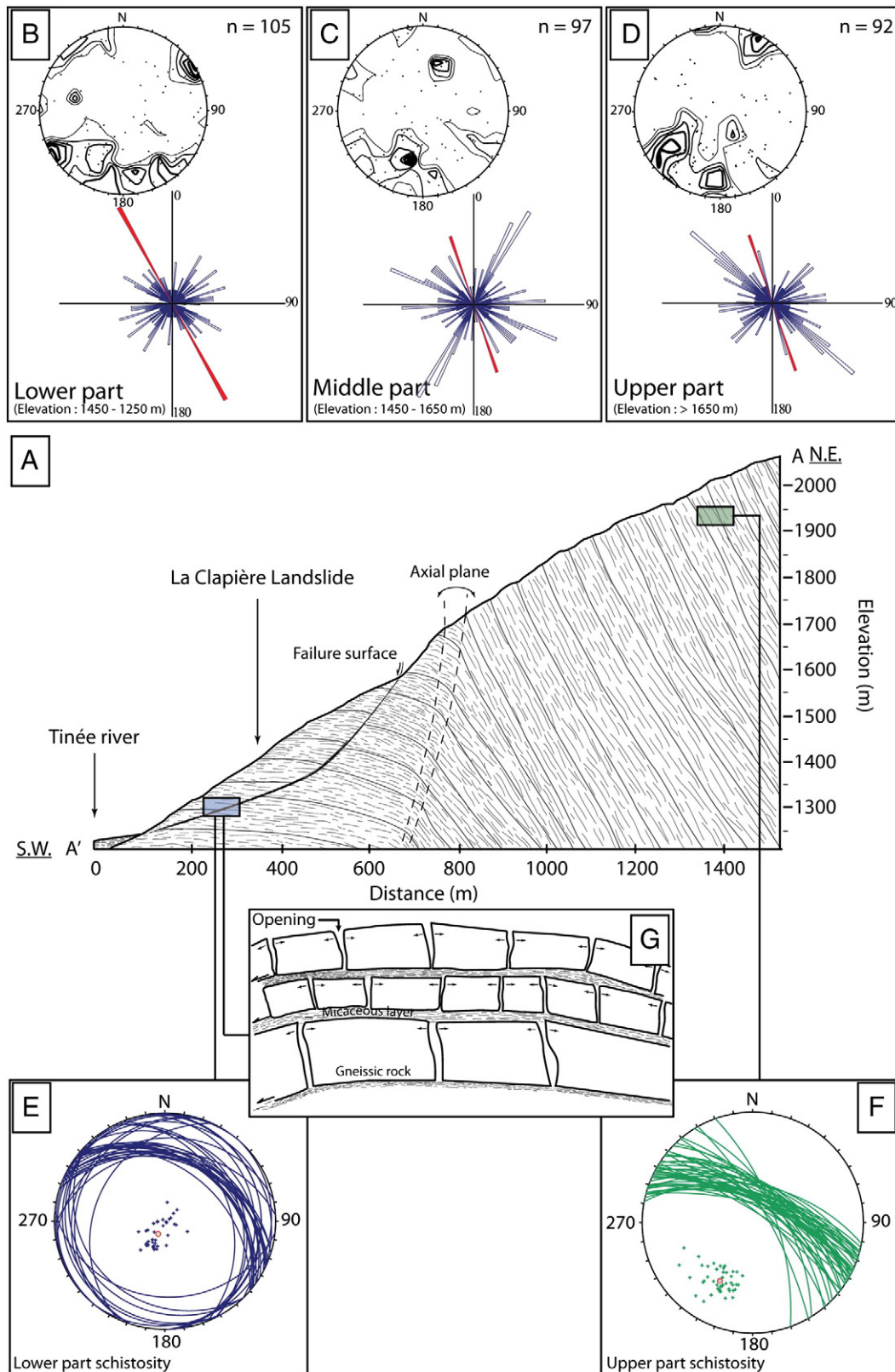
Fig. 3. A. Cross section of the La Clapière landslide along profile AA′ (Fig. 1), showing a schistosity of gneissic rocks. It is sub vertical in the North Eastern upper part, and sub horizontal in the lower part, of the landslide. The zone delimited by dashed line in (A) represents the schistosity fold axis strike. The thin brown layer represents the slip plane of the landslide. The Tinée River is located at the base of the landslide and is bounded by alluvial deposits. B, C, and D boxes show the fracturing style. The Wulff stereographic plot in lower hemisphere shows the poles to fracture planes and the related isodensity curves. In these boxes, the rose diagrams feature the statistics of fracture surface strikes. The orientation indicated by the red lines in (B–D) refers to fractures parallel to the valley. The Wulff stereonets in (E) and (F) show the orientations of schistosity in the lower and upper slope parts, respectively. The red circle shows the mean pole of schistosity on each canvas. (G) scheme shows the opening VP fractures due to the 'fold extrado' extension mechanism.
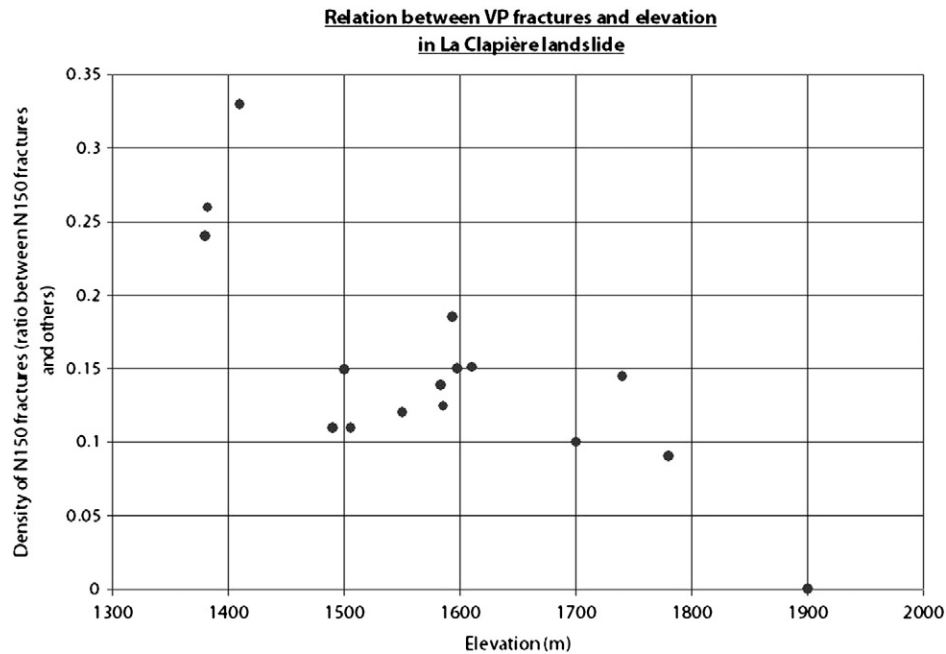
Fig. 4. Graph of the density of the valley parallel (VP) fractures versus elevation in the La Clapière landslide site.

Valley, ii) they correspond to distinct evolutionary stages of a deep seated landslide evolution, iii) they are located far from the N140°E mylonitic shear zones and hence far from any recent seismic activity (Jenatton et al., 2007; Sanchez et al., 2010a), and iv) they are located close to the villages. Therefore in addition to a purely scientific interest, these landslides are of importance for risk assessment.

In both cases, we selected about 80 outcrops located close to the landslides (Fig. 1). The volume of accessible outcrops for fracture documentation in both areas varies along slope from 1 m^3 to 100 m^3. In order to apply the same methodology of fracture description in both cases (along profiles AA′ and BB′ in Fig. 1), we defined a reference outcrop volume containing at least 10 fractures. This volume represents a cube of 8 m^3 (Fig. 2). We selected outcrops at different altitudes (Fig. 1) and present the results of fracture analysis and cleavage anisotropies (strike and dip) in Schmidt stereograms in lower hemisphere using INVDIR method of Angelier (1990).

In the lower part of the La Clapière area slope, it can be seen that schistosity dip is very low at shallow depth and increases abruptly at a depth of about 400 m to become sub-vertical at greater depth (Fig. 3). In this area the most abundant fracture family is oriented between N 140°E and N 150°E. This family is sub-vertical and almost parallel to the valley. The two other main fracture families are oriented N 030°E and N 120°E. In the middle part of slope, the schistosity is still sub-horizontal at shallow depth and sub-vertical at depths greater than 400 m. The fracture family trending N 030°E dominates, but the sub-vertical VP family is also present. This latter family is still encountered in the upper part of slope, but is much less abundant. In this area the schistosity is sub-vertical even at shallow depth and fractures are mainly oriented N 050°E. The density of the VP fractures thus decreases with altitude (Fig. 4).

A similar situation is observed in the Isola area. The schistosity is sub-horizontal at shallow depth in the lower and the middle part of slope, while it tends to be sub-vertical elsewhere at the massif's scale (Fig. 5). The abrupt change in schistosity dip from horizontal to vertical is also observed at a depth of about 400 m. The most abundant fractures in the lower part of slope are oriented N 130°E. They are sub-vertical and sub-parallel to the valley. The other fracture families are oriented N 020°E, N 100°E - N 115°E and N° 170°E. In the middle part of slope, the VP fractures are no longer present. In this part the main family is oriented N 115°E. In the upper part of slope,

the VP family dominates once again. The other present fracture sets are N 020° and N 070°. The density of the VP fractures decreases with altitude (Fig. 6), but not as strongly as in the La Clapière area (compare Figs. 4 and 6).

In both studied areas the tilting of schistosity delimitates folds under the two landslides at a depth of about 400 m. The lateral extend for the gravity-induced folds is estimated to be slightly larger than the width of the landslides (Fig. 1). The associated VP fractures are observed only close to the active landslides over a distance less than 200 m from them. No VP fracture clusters were observed in either of the studied areas that are characterised by rather uniform (or smoothly varying) fracture spacing. The latter ranges from 1 to 20 cm, increasing upwards along profiles. Unlike other fracture sets, the VP fractures have irregular (wavy) surfaces, do not possess any striae. The striae in the other fracture sets are compatible with regional Oligocene–Miocene right-lateral strike-slip tectonics, and are incompatible with some gravity motions. Finally, all observed VP fractures are opened and do not bear traces of mineralisation; they are therefore younger than the tectonic fracture sets filled with calcite or chlorite. From geometrical relationships and kinematics it appears that the VP fractures represent 'fold extrado'-like joints and that they are clearly related to the progressive tilting of schistosity (Fig. 3G).

3. Numerical modelling

3.1. Set-up

2-D plane-strain simulations were performed using finite-difference, explicit code FLAC3D and Hooke–Mohr–Coulomb constitutive model with zero hardening modulus (no strain softening or hardening) (see Chemenda et al., 2009 for more details of the constitutive formulation and model setup). Roller boundary conditions were imposed at vertical borders of the models (Fig. 7), while at the model bottom two types of conditions, roller and fixed were applied in different models. The model topography (free surface) is extracted from an SRTM file (referred to as SRTM_38_04). The numerical grid zone size (e.g. spatial resolution) varied from 150 m to 10 m. In the latter case the model has 110000 numerical zones. Given the dynamic relaxation technique implemented in Flac for accurate simulation of quasi-static deformation, the time-step is very small such that the model run requires about 8×10^5 steps, which
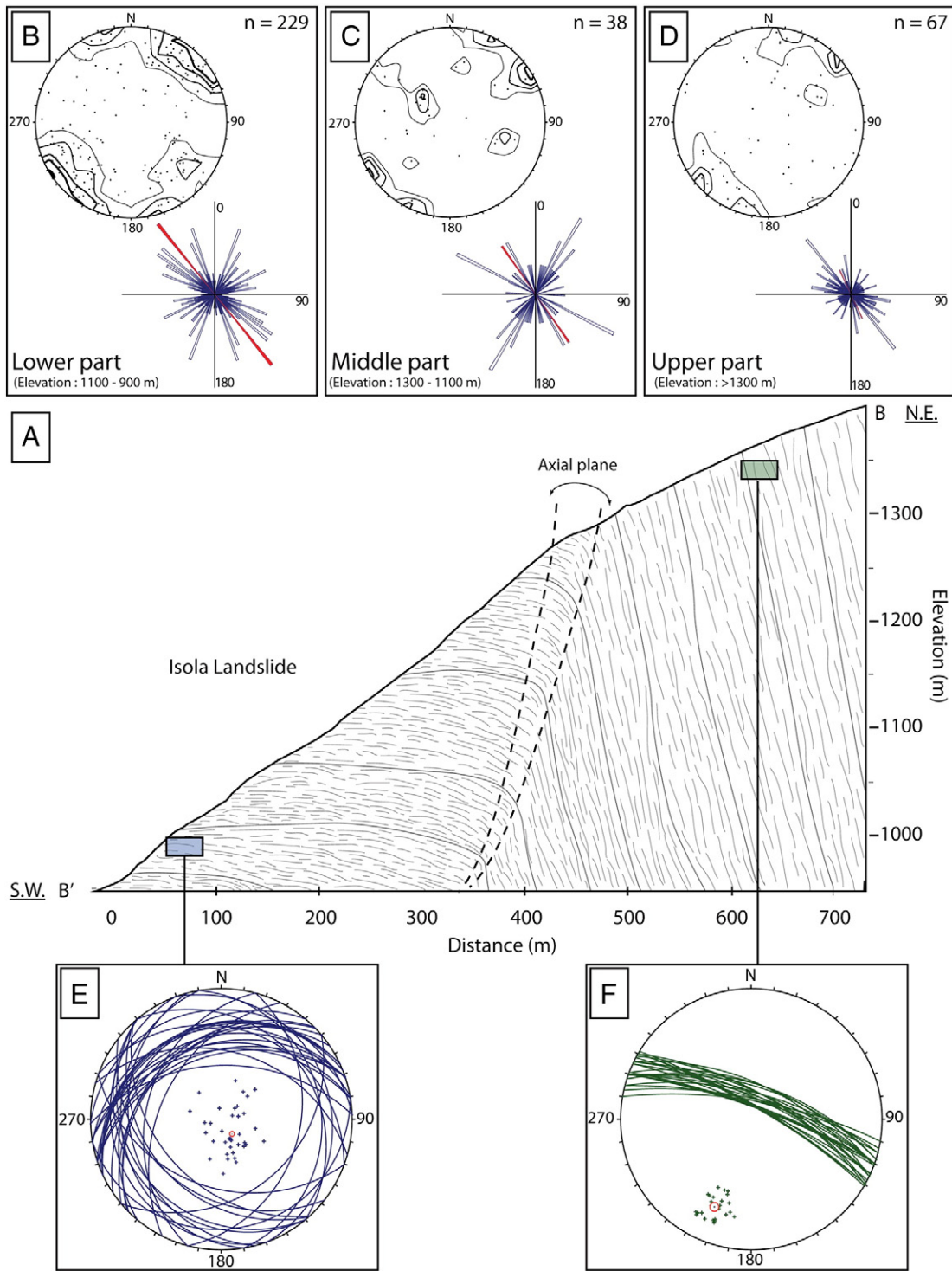
Fig. 5. (A) Cross section of the Isola landslide along profile BB′ (Fig. 1). Schistosity of gneissic rock is sub vertical in the North Eastern upper part of the landslide and sub horizontal in the lower part of the landslide. A zone delimited by the dashed line shows the schistosity fold axis strike. (B to D), The Wulff stereonet in lower hemisphere are plotted the poles to fracture planes and corresponding isodensity curves. In these boxes, the rose diagrams feature the statistics of fracture surface strikes. The orientation indicated by the red colour refers to fractures parallel to the valley. The Wulff stereonets of E and F boxes show the orientations of schistosity in the lower and upper slope parts, respectively. The red circle shows the mean pole of schistosity on each canvas.

takes about two days for calculation of the model with 10 m zone size on two quad-core processors.

The model is initially elastically equilibrated under the gravity force with the following parameter values: the Young modulus $E = 20$ GPa, the Poisson ratio $v = 0.23$, and the density $\rho = 2\,700$ kg/m^3 (Chemenda et al., 2009; Merrien-Soukatchoff et al., 2001; Willenberg, 2004). The internal friction angle ϕ is 30° according to

the experimental data (Hoek and Brown, 1997) and the previous modelling results (Chemenda et al., 2009). The initial cohesion c_{ini} was set to 10 MPa so that the initial (after equilibration) stress-state of the model in the most critical point was close to the yield surface, but still in the elastic domain. During cycling (a model evolution), c is incrementally reduced throughout the whole model, while ϕ is kept constant. Chemenda et al. (2009) have shown that in order to

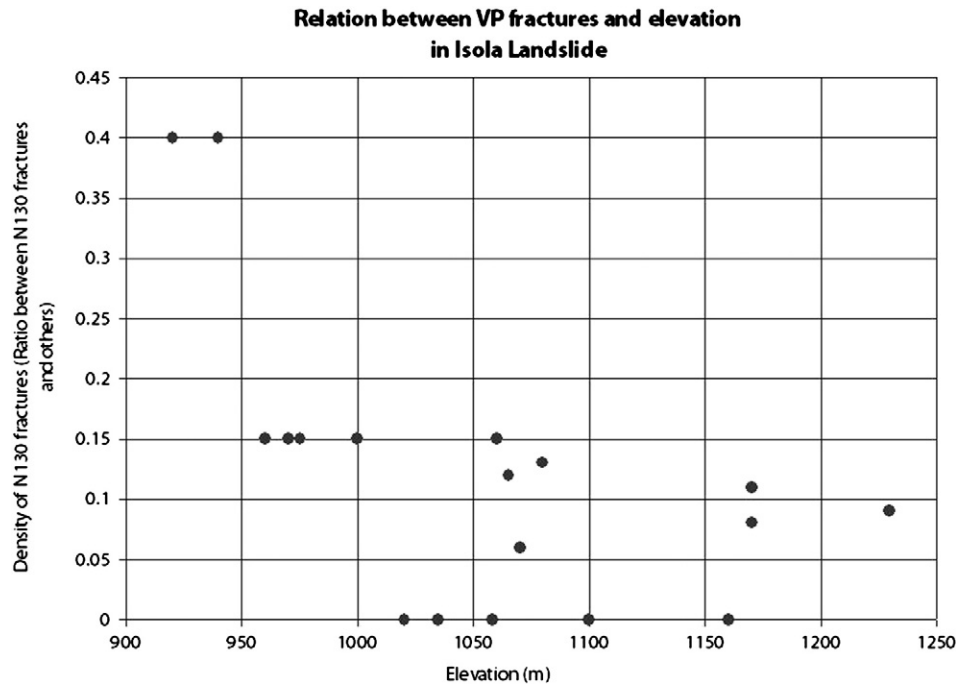**Relation between VP fractures and elevation
in Isola Landslide**

Fig. 6. Graph of the density of the VP fractures versus altitude for Isola landslide site.

maintain the model under quasi-static conditions and have stable results, the incremental reduction of the cohesion Δc must be less than $0.1c$ (where c is the current value of the cohesion during cycling). In the present models Δc was less than $0.01c$. The new reduction in cohesion must be applied when the inelastic deformation caused by the previous c reduction has ceased. We followed this procedure in the present modelling.

3.2. Results

Fig. 8a to i show the model presented in (Chemenda et al., 2009), but with additional evolutionary stages (8c and 8e) preceding the initiation of the "La Clapière" landslide, as well as with orientation of the principal stress directions (Fig. 8d). Roller boundary conditions were applied to the model bottom in this case. At the initial stages of the model evolution, the inelastic deformation concentrates at depth, under the summit zone where form two shear bands (normal faults) crossing the whole model from the base to the surface. Displacement along these faults causes sagging of the mountain crest. Then the inelastic deformation affects the lower part of the slope, resulting in the formation of a few smaller-scale deformation bands extending to depth of about 400 m (Fig. 8c). These bands are quasi vertical near the surface and curve with depth. Their number increases with deformation and new slope-parallel deformation bands appear at depths from 100 to 300 m (Fig. 8e). The inelastic deformation (material failure) along one of these latter bands evolves more rapidly than within the others. This band grows down- and up-slope at a depth of

about 100 m (Fig. 8f and i). It delimits a sliding unit corresponding to the La Clapiere landslide. The deep normal faulting in the thickest part of the model and the associated crest sagging remain active throughout the whole model evolution, but the displacement along the large-scale normal faults is more than two orders of magnitude lower than landsliding at shallow depth during the last stage of the model evolution in Fig. 8.

Fig. 9 presents the evolution of another model that differs from the previous one only by the condition imposed at the model bottom (fixed in all directions). The inelastic deformation starts in this case at some distance from the model bottom (Fig. 9a) and is followed by the formation of a set of deformation bands and a sagging of the mountain crest (Fig. 9b and e). At some stage, the inelastic deformation affects the lower part of the slope (Fig. 9b and c) and results in dense sub-vertical inelastic deformation bands. These bands propagate downwards and their number increases (Fig. 9e and f). Two bands sub-parallel to the surface form as well (Fig. 9f). The evolution of the inelastic deformation results in the "La Clapiere" landslide similar to the previous model. The two sets of inelastic deformation bands (sub-vertical and sub-parallel to the free surface) are oriented at 30° to the maximum principal stress (Fig. 9d) which is close to that predicted from the used Mohr–Coulomb constitutive model (see caption of Fig. 9).

In Fig. 10 we present two more models, both with fixed bottom. The model in Fig. 10a and b differs from the previous one only by the size of numerical zones (resolution), which is two times smaller (the number of grid zones is four times greater). The model in Fig. 10c and d has the same resolution as those in Figs. 8 and 9, but is three times thicker under the valley axis. It is seen that the evolution of these models is similar and both are similar to the model in Fig. 9.

4. Concluding discussion

4.1. Slope deformation predicted from numerical models

Since there are many uncertainties regarding the mechanical behaviour of the rocks at the slope scale and the boundary conditions, we wanted the models to be as simple as possible without introduction of any complications (heterogeneities) to fit the data. The models are initially homogeneous and evolve to a heterogeneous deformation and
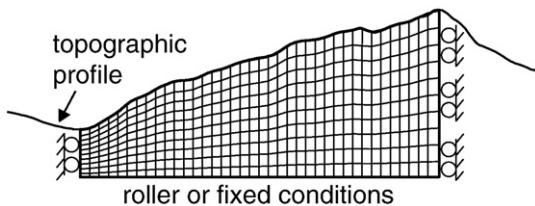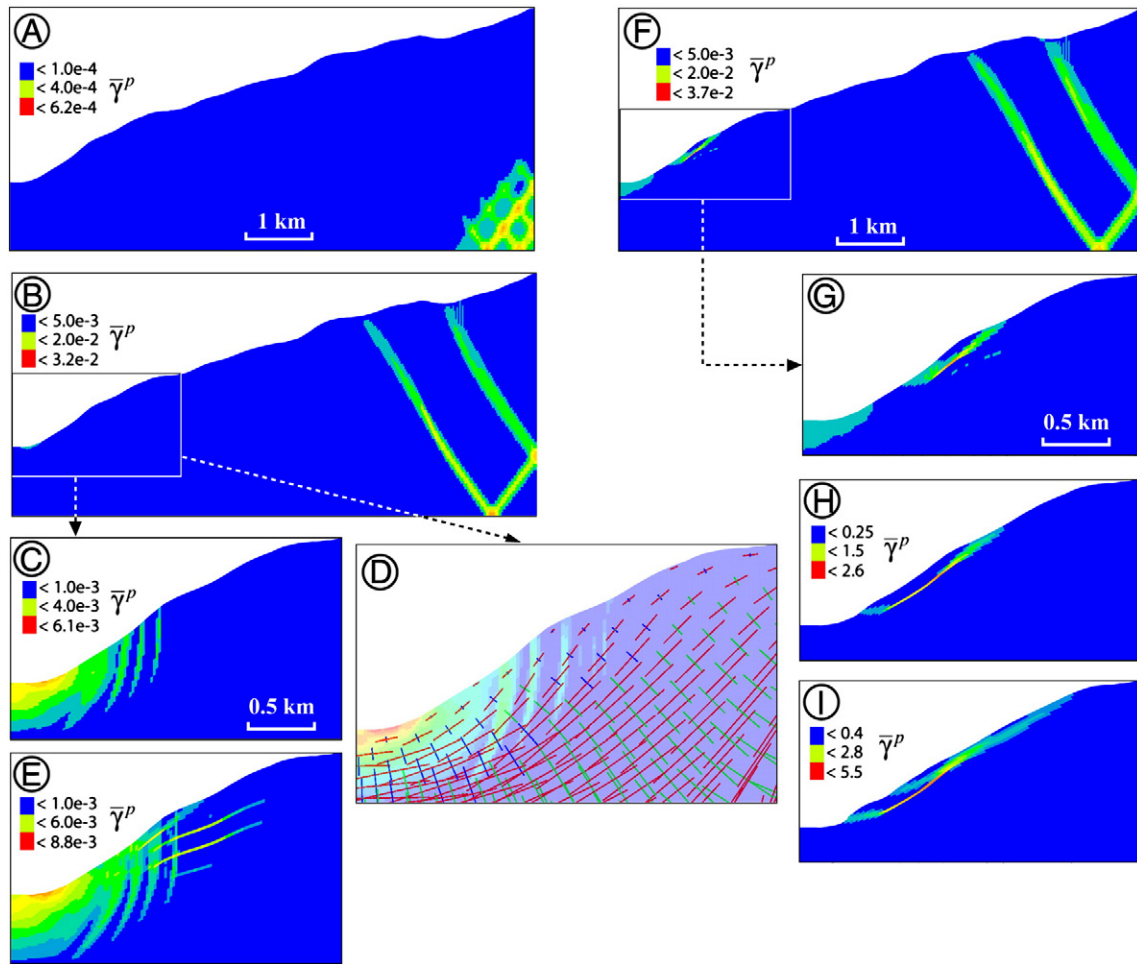

Fig. 7. Set up of numerical models and the grid geometry. The roller conditions are imposed along the vertical borders of the model. The model bottom is either fixed in all directions or subjected to roller conditions.

Fig. 8. Evolution of the pattern of accumulated inelastic shear deformation $\bar{\gamma}^p$ in the numerical model with roller conditions at the model surface (this model is from (Chemenda et al., 2009) with added evolutionary stages in c and e). Added is also the stress orientations (d) shown on the background on the semi-transparent $\bar{\gamma}^p$ pattern; red green, and blue lines correspond respectively to σ_1, σ_2, and σ_3 ($\sigma_1 > \sigma_2 > \sigma_3$, compressive stress is positive). The average grid zone size is 20 m; the total number of zones is ~30000.

failure only due to the imposed degradation of the material properties (reduction of the cohesion) that depends only on time. Roller (e.g. Guglielmi and Cappa, 2010; Merrien-Soukatchoff et al., 2001) or fixed (e. g. Apuani et al., 2007; Eberhardt et al., 2004) conditions at the model base are used by different authors. The reality likely is between these extreme cases. Therefore we tested the models with both types of conditions and it was shown that although the difference in the results exists, it is not crucial for this study. In all cases the inelastic deformation (material damage) is concentrated in the lower part of the slope at a certain stage of the process. The sub-vertical deformation bands with very small thrust offset (which does not exceed a few centimetres as follows from Fig. 9g) then form in this zone. The depth to which they extend is clearly boundary conditions-dependent: in the case of fixed model bottom (Figs. 9f, 10b and d), the depth (200 m) is almost twice smaller than in the models with roller conditions (Fig. 8c). In addition, in the latter case the bands curve with depth toward the valley axis (Fig. 8). It should be noted that although the above bands in the models have certain spacing, it is not representative of reality. This parameter is strongly dependent of the hardening modulus (Chemenda, 2007), which is very ill-constrained for real materials and in the presented models was arbitrary set to zero as it is usually done.

The orientation of the sub-vertical deformation bands in Figs. 8c, 9f, 10b and d coincides with the numerical grid lines, which may suggests that these bands are mesh-induced. However, the analysis of the stress orientations (Figs. 8d and 9d) shows that the obtained band orientation is close to that predicted from used Mohr–Coulomb

model as is demonstrated in Fig. 9d and explained in the caption to this figure. The principal stress orientations in Fig. 9d are also compatible with the orientation of the future (forming at later deformation stages) principal shear/sliding surface of the "La Clapière" landslide, which on the contrary, accommodates large shear displacement. Therefore the effect of the grid anisotropy is rather moderate. Note that the stress orientation in the models with different boundary conditions is considerably different (Figs. 8d and 9d).

The displacement along the deformation bands (normal faults) in the thickest part of the models is large. Their geometry also somewhat depends on the boundary conditions, although in all cases the displacement along them results in the crest sagging. The depth of origin of the valley axis-verging fault under the crest depends on the model thickness (the depth increases with the thickness as follows from the comparison of Figs. 9e and 10c) and to a certain degree, on the grid resolution (compare Figs. 9e and 10a). The orientation of normal faults obtained previously in the physical models (Bachmann et al., 2006; Chemenda et al., 2005) is closer to the case with fixed bottom than with roller conditions, but do not coincide with numerical result. The reason is that in the physical experiments, the conditions at the model bottom are not controlled during the deformation and certainly do not correspond to the total coupling. The internal friction of the model material is also lower that the value assumed in the present simulations.

Our models show that the explicit introduction of pre-existing tectonic fractures or use of equivalent continuum approach (Sitharam
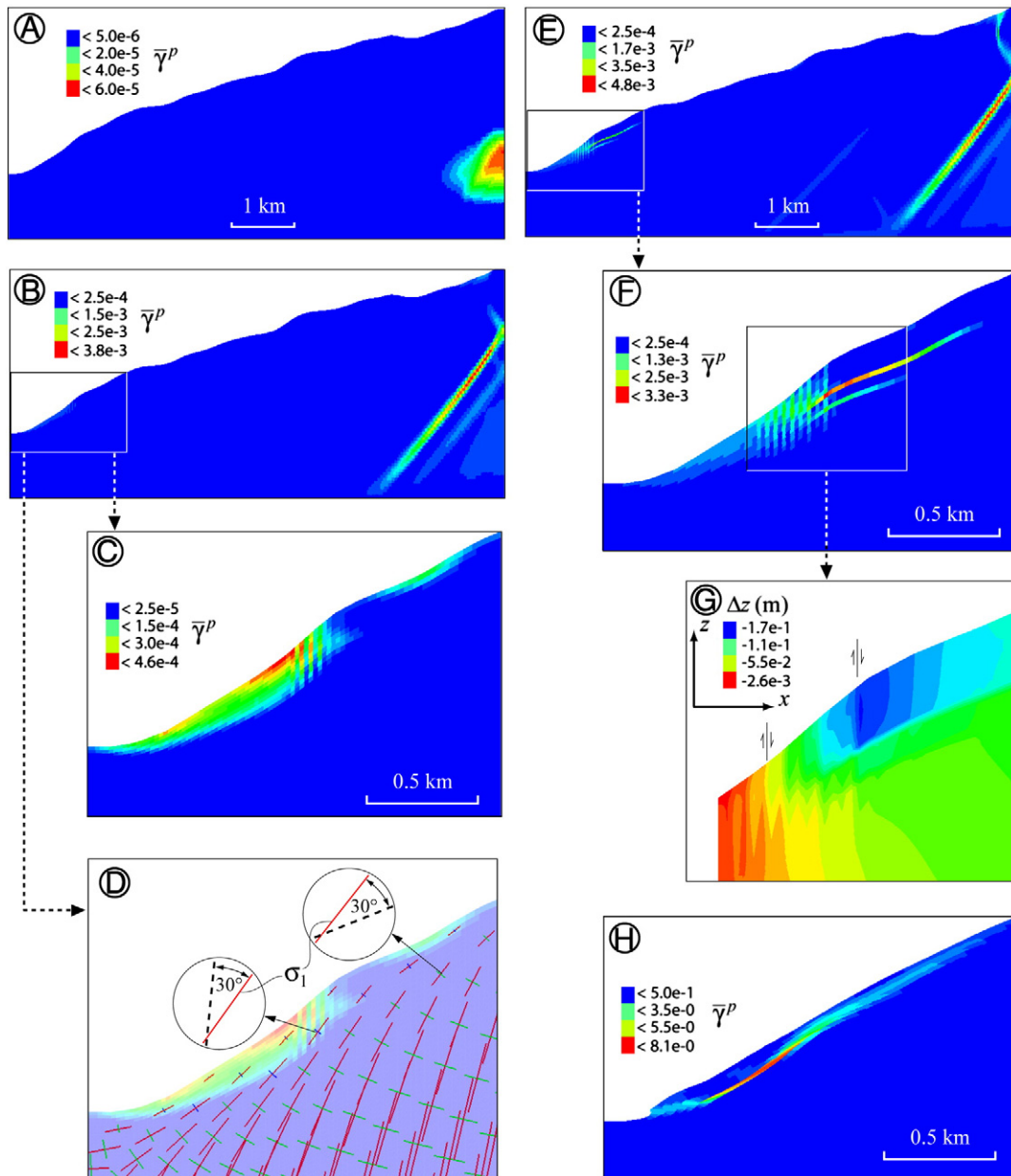
Fig. 9. Evolution of the model with bottom fixed in all direction. (a, b, c, e f, and d) Successive stages of evolution of $\bar{\gamma}^p$ pattern; (d) orientation of principal directions shown on the background on the semi-transparent $\bar{\gamma}^p$ pattern; red green, and blue lines correspond respectively to σ_1, σ_2, and σ_3. The insets in circles zoom in the σ_1 orientations (red lines) in two point of the model and the orientation of potential failure/deformation localisation (dashed lines) plans predicted from the Mohr-Coulomb model. The angle ψ between this plan and the σ_1 direction should be $\psi = \pi/4 - \phi/2 = 30°$. (g) Vertical displacement Δz at stage (f). The average grid zone size is 20 m; the total number of zones is ~30000.

and Madhavi Latha, 2002; Sitharam et al., 2001) is not necessary to explain the development of the La Clapière landslide. To a first approximation, the slope destabilization does not seem to be sensitive to structural and mechanical heterogeneities (that are usually not well constrained), at least in two dimensions. Eberhardt et al. (2004) arrived to the same conclusion from the models of the Randa landslide. These authors have also obtained both vertical and surface parallel fractures using the code ELFEN. The principal difference with our results is that the vertical fractures in their model are tensile (i.e., form under tensile stress σ_3 reaching the tensile strength of the material). In our models σ_3 is always compressive except locally at very shallow depths at late stages of the slope fracturing. The large tensile stresses in the Eberhardt et al. (2004) models are possibly caused by the procedure of an apparently instantaneous glacial unloading/rebound, which could have generate high dynamic tensile stresses (the deformation of our models is maintained

quasi-static as described in Section 3.1). The considerable difference in our results can also be related to the difference in topography in the La Clapière and Randa landslides (in the latter case it is stepper).

4.2. Comparison with field observations and constraints on the landslide initiation processes

Field observations have revealed a family of vertical, valley-parallel (VP) fractures in the vicinity of both the La Clapière and Isola landslides in the lower parts of the slopes. These VP fractures are clearly related to the decrease in schistosity dip corresponding to 'folds' or cleavage bends around the two landslides to depth of about 400 m. The VP fractures appear as 'fold-extrado' joints. Since these features are observed only in the vicinity of the landslides, they are most likely gravity-induced (as was previously concluded based on
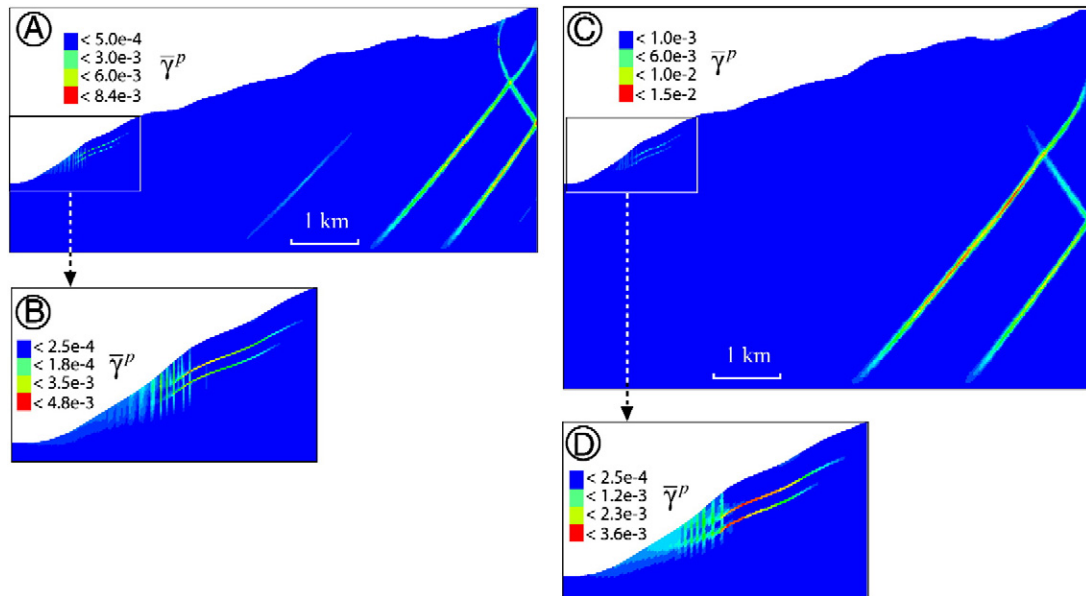
Fig. 10. Two models (a, b) and (c, d) with fixed bottom having different size and resolution. (a, b) The size is the same of the two previous models: the thickness under the valley axis is 1 km. The grid zone size is 10 m, i.e., twice smaller than in the previous models. The total number of drip zones is 110000. (c, d) The model thickness under the valley axis is 3 km. The grid zone size is 20 m, and the total number of grid zones is 80000.

the numerical modelling results by Chemenda et al. (2009)) and are not caused by the Oligocene–Miocene thrust tectonics as was suggested by Gunzburger and Laumonier (2002). In agreement with previous field (Guglielmi et al., 2005) and modelling (Chemenda et al., 2009) studies, the depth of the fold axis was found to be more than two times greater than that of the basal slip plane of the landslides. It is meaningful that the depth of the folding axis measured in the field approximately coincides with the depth to which the inelastic deformation occurs in the numerical models. This suggests that the gravity-induced damage (inelastic deformation) in the lower part of slope results in a very considerable reduction of the strength of material and its down slope flow. This rapid material weakening can be caused by the increased permeably of the damaged material and the related acceleration in chemical weathering. The flow results in the tilting/folding of the pre-existing fabrics and the VP fracturing and then, in the formation of a localized slope-parallel shear plane giving start to the landslide itself in the upper part of the weakened volume. This scenario is to be confirmed based on both a detailed characterisation of the material weathering/weakening in relation with its mechanical damage and on the numerical modelling taking into account such a relation.

In conclusion, the pattern of pre-existing anisotropies in the rock mass (schistosity or bedding) and associated fracturing in the areas on potential landsliding provide important information for evaluating the damage state and the risk of gravitational destabilisation of slopes. In the case of the Upper Tinée Valley, several stages of landslide development could be identified from the distribution of such features. (1) In the Isola site, tilting of schistosity and the VP fracturing are present, but no localised landslide surface has been formed. This area corresponds therefore to the incipient landsliding. (2) In the La Clapière landslide, both the tilting and the VP fracturing are observed as well, but they are more pronounced and in addition there is an active localised landsliding. The location and intensity of the schistosity folding and the associated VP fracturing can thus serve a basis for estimation of both the surface and the volume that could be affected by the future landslide.

Acknowledgements

References

Angelier, J., 1990. Inversion of field data in fault tectonics to obtain the regional stress: a new rapid direct inversion method by analytical means. Geophysical Journal International 103, 363–376.

Apuani, T., Masetti, M., Rossi, M., 2007. Stress-strain-time numerical modelling of a deepseated gravitational slope deformation: preliminary results. Quaternary International 171–172, 80–89.

Bachmann, D., Bouissou, S., Chemenda, A., 2006. Influence of large scale topography on gravitational rock mass movements: new insights from physical modeling. Geophysical Research Letters 33, L21406. doi:10.1029/2006GL028028.

Bachmann, D., Bouissou, S., Chemenda, A., 2009. Analysis of massif fracturing during deep seated gravitational slope deformation by physical and numerical modeling. Geomorphology. doi:10.1016/j.geomorph.2007.09.018.

Bigot-Cormier, F., Braucher, R., Bourlès, D., Guglielmi, Y., Dubar, M., Stéphan, J.-F., 2005. Chronological constraints on processes leading to large active landslides. EPSL 235, 141–150.

Bogdanoff, S., 1986. Evolution de la partie occidentale du massif cristallin externe de l'Argentera. Place dans l'arc alpin. Géologie de France 4, 433–453.

Bois, T., Bouissou, S., 2010. Influence of tectonic fractures zones on gravitational rock slope failures: new insights from 2-D physical modeling. Journal of Geophysical Research 115, F03009. doi:10.1029/2009JF001403.

Bois, T., Bouissou, S., Guglielmi, Y., 2008. Influence of major inherited faults zones on gravitational slope deformation: a two-dimensional physical modelling of the La Clapière area (Southern French Alps). EPSL. doi:10.1016/j.epsl.2008.06.006.

Casson, B., Delacourt, C., Allemand, P., 2005. Contribution of multi-temporal remote sensing images to characterize landslide slip surface—application to the La Clapière landslide (France). Natural Hazards and Earth System Sciences 5, 425–437.

Chemenda, A., 2007. The formation of shear-band/fracture networks from a constitutive instability: theory and numerical experiment. Journal of Geophysical Research 112, B11404. doi:10.1029/2007JB005026.

Chemenda, A., Bouissou, S., Bachmann, D., 2005. 3-D physical modeling of deepseated landslides: new technique and first results. Journal of Geophysical Research 110, F04004. doi:10.1029/2004JF000264 No. F4.

Chemenda, A., Bois, T., Bouissou, S., Tric, E., Bachmann, D., 2009. Numerical modelling of the gravity-induced destabilization of a slope: the example of the La Clapière landslide, southern France. Geomorphology. doi:10.1016/j.geomorph.2009.02.025.

Corsini, M., Ruffet, G., Caby, R., 2004. Alpine and late hercyniangeochronological constraints in the Argentera Massif (Western Alps). Eclogae Geolicae Helvetiae 97, 3–15.

Delteil, J., Stephan, J.F., Attal, M., 2003. Control of Permian and Triassic faults on Alpine basement deformation in the Argentera massif (external southern French Alps). Bulletin de la Société Géologique de France 174, 55–70.

Eberhardt, E., Stead, D., Coggan, J., 2004. Numerical analysis of initiation and progressive failure in natural rock slopes: the 1991 Randa rockslides. International Journal of Rock Mechanics and Mining Sciences 41, 69–87. doi:10.1016/ S1365-1609(03)00076-5.

El Bedoui, S., Bois, T., Jomard, H., Sanchez, G., Lebourg, T., Tric, E., Guglielmi, Y., Bouissou, S., Chemenda, A., Rolland, Y., Corsini, M., Pérez, J.L., 2011. Paraglacial gravitational deformations in the SW Alps: a review of field investigations, [10]Be cosmogenic dating and physical modeling. Geological Society, London, Special Publications 351, 11–25.

Follacci, J.P., 1987. Les mouvements du versant de La Clapière à Saint Étienne de Tinée (Alpes Maritimes). Bulletin de Liaison des Laboratoires des Ponts et Chaussées 220, 107–109.

Follacci, J.P., 1999. Seize ans de surveillance du glissement de La Clapière (Alpes Maritimes). Bulletin de Liaison des Laboratoires des Ponts et Chaussées 220, 35–51.

Guglielmi, Y., Cappa, F., 2010. Regional-scale relief evolution and large landslides: insights from geomechanical analyses in the Tinée Valley (southern French Alps). Geomorphology. doi:10.1016/j.geomorph.2009.11.016.

Guglielmi, Y., Vengeon, J.-M., Bertrand, C., Mudry, J., Follacci, J.-P., Giraud, A., 2002. Hydrochemistry: an investigation tool to evaluate infiltration into large moving rock masses (case study of La Clapière and Séchilienne alpine landslides). Bulletin of Engineering Geology and the Environment 61, 311–324.

Guglielmi, Y., Cappa, F., Binet, S., 2005. Coupling between hydrogeology and deformation of mountainous rock slopes: insights from La Clapière area (southern Alps, France). Comptes Rendus Geosciences 337, 1154–1163.

Gunzburger, Y., Laumonier, B., 2002. Origine tectonique du pli supportant le glissement de terrain de la Clapière (NordOuest du massif de l'Argentera–Mercantour, Alpes du Sud, France) d'après l'analyse de la fracturation. Comptes Rendus Geosciences 334, 415–422.

Hajiabdolmajid, V., Kaiser, P.K., 2002. Slope stability assessment in strain-sensitive rocks. EUROCK 2002, Proceedings of the ISRM International Symposium on Rock Engineering for Mountainous Regions, Funchal, Madeira, pp. 237–244.

Hall, K., André, M.F., 2001. New insights into rock weathering from high-frequency rock temperature data: an Antarctic study of weathering by thermal stress. Geomorphology 41, 23–35.

Hoek, E., Brown, E.T., 1997. Practical estimates of rock mass strength. International Journal of Rock Mechanics and Mining Sciences 8, 1165–1186.

Jenatton, L., Guiguet, R., Thouvenot, F., Daix, N., 2007. The 16,000-event 2003–2004 earthquake swarm in Ubaye (French Alps). Journal of Geophysical Research 112, B11304. doi:10.1029/2006JB004878.

Jomard, H., 2006. Analyse multi-échelles des déformations gravitaires du Massif de l'Argentera Mercantour. Ph.D Thesis, Departement des sciences de la terre et de l'univers, Univ. Nice Sophia Antipolis, Nice, France, 246 pp.

Kaneko, K., Otani, K.J., Noguchi, Y., Togashiki, N., 1997. Rock fracture mechanics analysis of slope failure. In: Asaoka, A., Adachi, T., Oka, F. (Eds.), Deformation and Progressive Failure in Geomechanics. Elsevier, New York, pp. 671–676.

Merrien-Soukatchoff, V., Quenot, X., Guglielmi, Y., 2001. Modélisation par éléments distincts du phénomène de fauchage gravitaire. Application au glissement de La Clapière (Saint-Etienne-de-Tinée, Alpes Maritimes). Rev. Fr. Géotech. 95/96, 133–142.

Migon, P., Lidmar-Bergstroem, K., 2002. Deep weathering through time in central and northwestern Europe: problems of dating and interpretation of geological records. Catena 49, 25–40.

Petley, D., 1996. The mechanics and landforms of deep-seated landslides. In: Anderson, M.G., Brooks, S.M. (Eds.), Advances in Hillslope Processes. John Wiley, Hoboken, N. J, pp. 823–834.

Sanchez, G., Rolland, Y., Schreiber, D., Giannerini, G., Corsini, M., Lardeaux, J.-M., 2010a. The active fault system of SW Alps. Journal of Geodynamics 49, 296–302. doi:10.1016/j.jog.2009.11.009.

Sanchez, G., Rolland, Y., Corsini, M., Braucher, R., Bourlès, D., Arnold, M., Aumaître, G., 2010b. Relationship between tectonics, slope instability and climate change: cosmic ray exposure dating of active faults, landslides and glacial surfaces in the SW Alps. Geomorphology 117, 1–13. doi:10.1016/j.geomorph.2009.10.019.

Sanchez, G., Rolland, Y., Schneider, J., Corsini, M., Oliot, E., Goncalves, P., Verati, C., Lardeaux, J.-M., Marquer, D., 2011a. Dating low-temperature deformation by 40Ar/39Ar on white mica, insights from the Argentera-Mercantour Massif (SW Alps). Lithos 125 (1–2), 521–536.

Sanchez, G., Rolland, Y., Corsini, M., Jolivet, M., Brichaud, S., Carter, A., 2011b. Exhumation controlled by transcurrent tectonics: the Argentera-Mercantour massif (SW Alps). Terra Nova 23, 116–126.

Scavia, C., 1995. A method for the study of crack propagation in rock structures. Geotechnique 45, 447–463.

Sitharam, T.G., Madhavi Latha, G., 2002. Simulation of excavation in jointed rock masses using a practical equivalent continuum approach. International Journal of Rock Mechanics and Mining Sciences 39, 517–525.

Sitharam, T.G., Sridevi, J., Shimizu, N., 2001. Practical equivalent continuum characterization of jointed rock masses. International Journal of Rock Mechanics and Mining Sciences 38, 437–448.

Willenberg H., 2004. Geologic and Kinematic model of a complex landslide in crystalline rock (Randa, Switzerland), Ph.D Thesis, Swiss Federal Institute of Technology, Zurich, 161 pp.